DA: 1X263302D212
AMCMS Code: 523B.12.1710000
HDL Proj: 63561

HDL-TR-1581

NORMAL MODE ANALYSIS OF A FUZE SUPPORT STRUCTURE USING NASTRAN (PART I)

by

William L. Fourney
John T. Crawley
R. Richard Palmisano

April 1972

U.S. ARMY MATERIEL COMMAND
HARRY DIAMOND LABORATORIES
WASHINGTON, D.C. 20438

UNCLASSIFIED
Security Classification

DOCUMENT CONTROL DATA - R & D

(Security classification of title, body of abstract and indexing annotation must be entered when the overall report is classified)

1. ORIGINATING ACTIVITY (Corporate author)
Harry Diamond Laboratories
Washington, D.C. 20438

2a. REPORT SECURITY CLASSIFICATION
Unclassified

2b. GROUP

3. REPORT TITLE
NORMAL MODE ANALYSIS OF A FUZE SUPPORT STRUCTURE USING "NASTRAN" (PART I)

4. DESCRIPTIVE NOTES (Type of report and inclusive dates)

5. AUTHOR(S) (First name, middle initial, last name)
William L. Fourney, John T. Crawley, R. Richard Palmisano

6. REPORT DATE	7a. TOTAL NO. OF PAGES	7b. NO. OF REFS
April 1972	40	0

8a. CONTRACT OR GRANT NO.	9a. ORIGINATOR'S REPORT NUMBER(S)
b. PROJECT NO. DA:1X263302D212	
c. AMCMS Code: 523B.12.1710000	9b. OTHER REPORT NO(S) (Any other numbers that may be assigned this report)
d. HDL Proj: 63561	

10. DISTRIBUTION STATEMENT
Approved for public release; distribution unlimited.

11. SUPPLEMENTARY NOTES	12. SPONSORING MILITARY ACTIVITY
	U.S. Army MICOM

13. ABSTRACT

A support structure for a propsed guided missile electronic fuze was designed with the aid of the NASA Structural Analysis (NASTRAN) finite element structural analysis program. Two differently mounted mock-up fuze models were fabricated and tested under a sinusoidal 2-g load applied in the transverse, as well as the axial, direction. Good correlation was obtained between the values of natural frequency measured experimentally and those obtained from the digital computer program.

14. KEY WORDS	LINK A		LINK B		LINK C	
	ROLE	WT	ROLE	WT	ROLE	WT
Finite element vibration analysis	8	3				
NASTRAN	8	3				
Vibration analysis of missile fuze structure	8	3				
Structural mock-up evaluation	8	3				

ABSTRACT

A support structure for a proposed guided missile electronic fuze was designed with the aid of the NASA Structural Analysis (NASTRAN) finite element structural analysis program. Two differently mounted mock-up fuze models were fabricated and tested under a sinusoidal 2-g load applied in the transverse, as well as the axial, direction. Good correlation was obtained between the values of natural frequency measured experimentally and those obtained from the digital computer program.

CONTENTS

ABSTRACT..... 3

1. INTRODUCTION..... 7

2. COMPUTER-AIDED DESIGN..... 7

3. EXPERIMENTAL STUDY.....12

3.1 Model Description.....12
3.2 A-1 Model Tests.....15
3.3 F-1 Model Tests.....18

4. RESULTS.....18

5. CONCLUSIONS.....19

6. RECOMMENDATIONS.....21

APPENDIX A. INPUT DATA TO NASTRAN FOR FUZE MODEL A-1.....28

APPENDIX B. SAMPLE OF NASTRAN OUTPUT FOR FUZE MODEL A-1.....31

TABLES

I. Natural frequencies obtained for model A-1.....12
II. Natural frequencies obtained for model F-1.....12
III. Natural frequencies obtained for model A-3.....12
IV. Fuze mock-up weight.....15
V. Experimentally obtained natural frequencies (Hz).....19

FIGURES

1. Aft-mounted fuze structural model (A-1)..... 8
2. Fore-mounted fuze structural model (F-1)..... 8
3. Cross section of legs and struts for A-1 and F-1 structural mock-up models..... 9
4. Cross section of legs and struts for A-3 mathematical model. 9
5. Aft-mounted pad..... 9
6. Fore-mounted pad..... 9
7. NASTRAN mathematical model for A-1 model.....11
8. Structural mock-up of fuze components.....13
9. Structural mock-up of fuze components.....14
10. Structural fuze model showing dummy component arrangement, center of gravity, and accelerometers.....15
11. Structural fuze model showing dummy component arrangement, center of gravity, and accelerometers.....16
12. Fuze structural mock-up A-1 on shaker adapter plate.....17
13. Fuze structural mock-up F-1 on shaker adapter plate.....17
14. Fuze structural mock-up A-1 ready for vibration test.....20
15. Vibration test setup for Z-axis exitation of A-1 fuze mock-up mock-up.....20
16. Vibration test setup for transverse exitation of A-1 fuze mock-up.....21
17-25. Response of models A-1 and F-1 to 2-g sinusoidal input.....23-27

1. INTRODUCTION

A design study was made of a guided missile electronic fuze support structure. The structure was required to carry the loads developed during all missile environments and to have its lowest natural frequency as high as possible.

This natural frequency was intended to be high enough to insure that driving forces at this frequency would not be encountered during the life of the missile. On the other hand, if the natural frequency and internal damping were high enough, even though the driving forces were at frequencies near the structure's natural frequency, the transmissibility would be low enough to prevent the occurrence of large displacements.

The basic geometry of the fuze housing was initially assumed to be a rectangular box, 5 x 5 x 6 in. The total weight of the fuze and supporting structure was 10 lb, with 3 lb being allotted for the structure itself.

There were two phases of the design study. Phase one was a computer-aided analytical study of proposed configurations that utilized the NASA Structural Analysis (NASTRAN) digital computer program for finite element analysis of structures. Phase two was an experimental study of two structures tested to obtain results for comparison with the values obtained from phase one.

When the study began, the orientation of the rectangular fuze box with respect to the missile launch axis had not been determined, nor had it been decided whether the fuze would be attached to the fore or aft side of the 13-in. inner diameter bolting ring; the bolting ring was already part of the missile structure. A more desirable strut span was possible by the aft mounting than by the fore mounting procedure.

For these reasons two different orientations and two different mounting adapters were studied. In particular, analyses were undertaken assuming box orientations with both the five- and six-in. dimension in the direction of the missile axis.

Experimentally, two different types of mounting pads were investigated: one for forward mounting of the fuze, and the other for aft mounting. The letters A and F are used to designate aft and fore mounting, respectively. The numbers 1 and 3 are used to designate the six-in. (fig. 1 and 2) and the five-in. dimension oriented in the direction of the missile axis, respectively.

2. COMPUTER-AIDED DESIGN

The NASTRAN computer program for finite element analysis of structures was utilized to design the fuze support structure. NASTRAN is a finite element computer program for structural analysis of almost every kind of structure and type of construction. Structural elements are provided for specific representation of the more common types of construction, including rods, beams, shear panels, plates, and shells of revolution. Composite types of construction, such as the fuze structure analyzed in this report, are treated by combinations of these elements or by the use of "general" elements tailored to a specific requirement. Two of the formats available with the program, the static analysis format (Format 1) and the normal mode analysis (Format 3), were used in the design process.

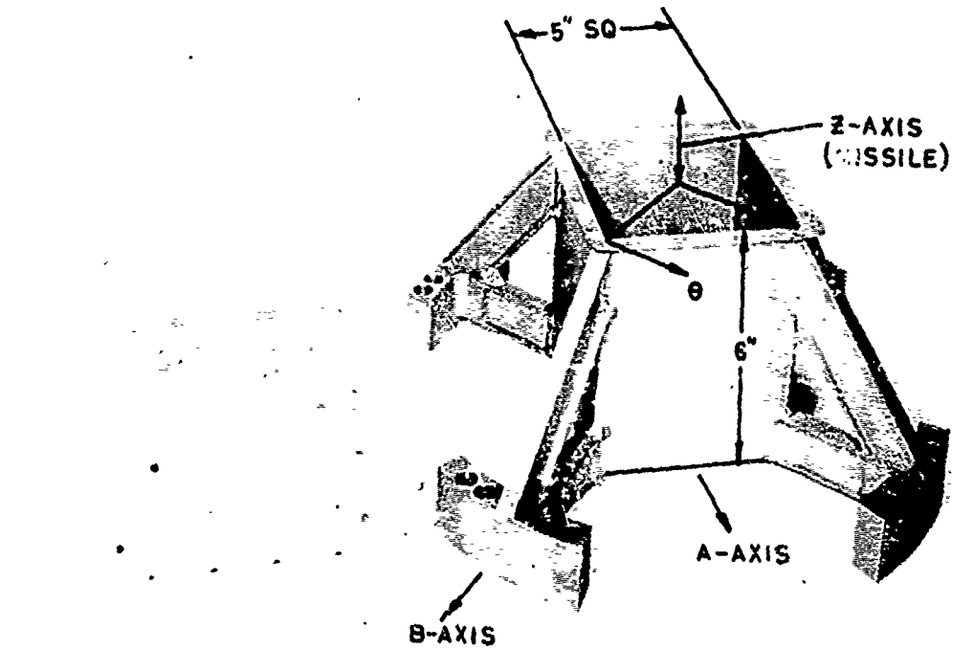

Figure 1. Aft-mounted fuze structural model (A-1).

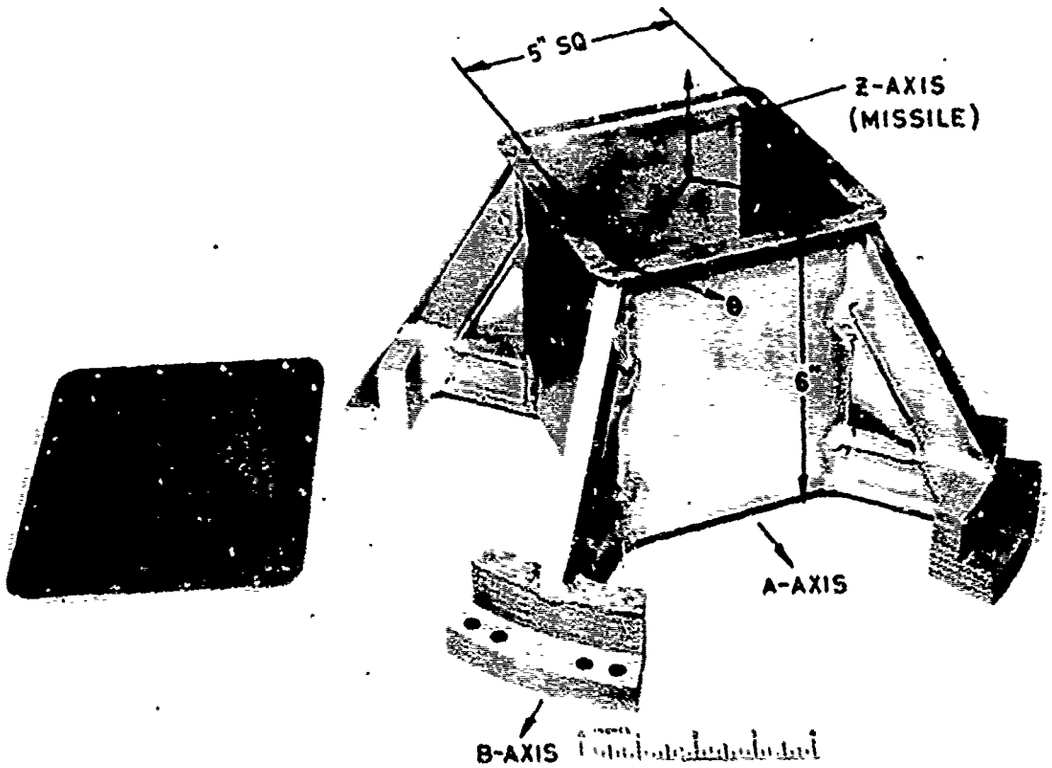

Figure 2. Fore-mounted fuze structural model (F-1).

The static format was used to determine the stress level in the structure due to an equivalent 50-g launch load, and the normal mode analysis was used to determine the mode shapes and natural frequencies of the fuze support.

Figure 1 shows the aft-mounted model (A-1) that was studied experimentally. The box portion of the fuze was connected to four pads, which bolt to the mounting ring in the missile, by four struts whose cross section was an I-beam, and by four shorter legs of similar cross section (fig. 3, 5, and 6). The various fuze components were arranged in a predetermined fashion inside the box, and 6-lb/ft^3 polyurethane foam was used to encapsulate these in place. Figure 7 shows one quarter of the mathematical model used in the NASTRAN program for the aft-mounted support structure. It was necessary to use only one quarter of the structure in the analytical investigation, since symmetry about two perpendicular planes exists for the A-1 case.

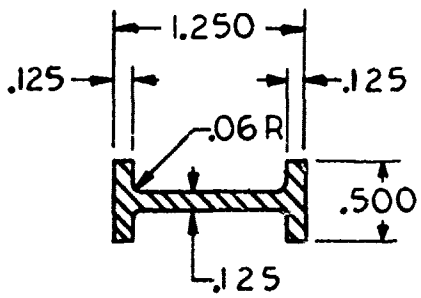

Figure 3. Cross section of legs and struts for A-1 and F-1 structural mock-up models.

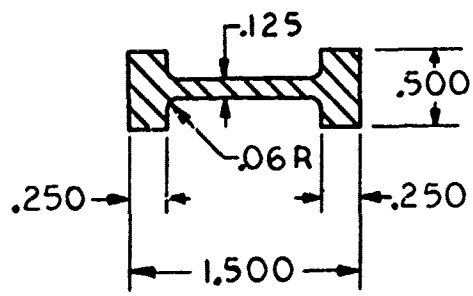

Figure 4. Cross section of legs and struts for A-3 mathematical model.

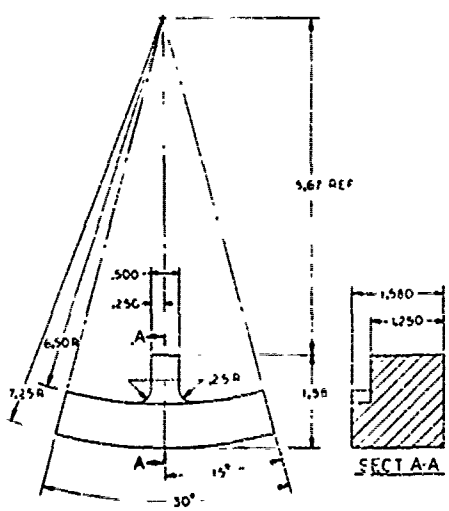

Figure 5. Aft-mounted pad.

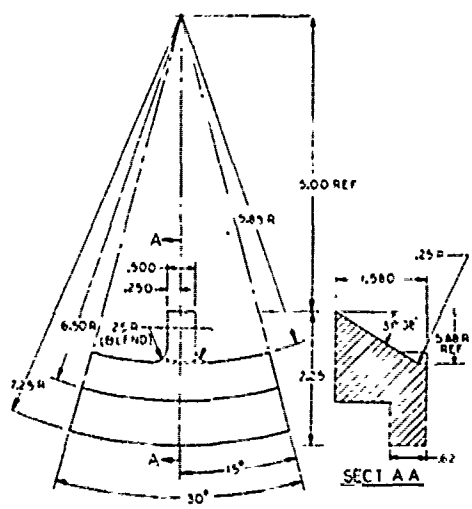

Figure 6. Fore-mounted pad.

In figure 7, one and two digit numbers refer to grid points. Numbers 101 through 148 identify homogeneous quadralateral membrane and bending elements, 201 through 207 identify simple beam elements, and 301 through 309 identify rod elements. The quadralateral elements are capable of resisting moments and forces applied in any direction with the exception that they cannot withstand a moment applied about an axis normal to the large faces of the element. The rod elements can withstand only tension or compression forces and torsional moments, whereas the bar elements can withstand axial forces, shear in two directions, as well as bending and torsional moments.

The quadralateral elements were used to represent the box walls that were 1/16-in. thick and made from 6061-T6 aluminum alloy. The bar elements were used to represent the struts and the legs and were taken to be of "I" cross section. These also were made of 6061-T6 aluminum. The mounting pads were not included in the mathematical model, but their effect was assumed to constrain grid points 23 and 48 (the ends of the legs and struts) to such an extent that no displacements or rotations were permitted.

The rod elements represent the polyurethane foam and were taken to be oriented only in the Z-direction. In reality, they should be oriented in all directions, but there was no convenient NASTRAN element to represent this continuum situation. To include other rods in the X and Y directions would have made it necessary to have a large number of additional grid points and would have significantly increased the computer time required. The total area of the rods equalled the area of the top face of the box. When viewing the computer results with this mathematical model, it will be necessary to remember that the deflections obtained in the X and Y directions will be larger than expected, since the stiffness of the polyurethane foam in these directions was neglected.

Typical input and output from the computer is shown in the appendix for normal mode analysis format and for the model shown in figure 4.

The weight of the fuze box and internal support structure was approximately 1 lb, leaving 6 lb for the weight of the simulated fuze components. These 6 lb were distributed in the mathematical model as follows: The top and bottom of the can were each assumed to carry 1.5 lb, and each of the four sides was assumed to carry 0.75 lb. This weight was distributed uniformly on each of the areas in question and was entered into the computer as nonstructural mass. This particular distribution was chosen because the foam material was thought to be capable of distributing the load uniformly and was capable of transmitting shear loading to the box sides. The center of gravity of the simulated fuze components was, therefore, assumed to lie at the geometric center of the box. Three different configurations were investigated on the computer:

1. Model A-1; the aft-mounted box with the 6-in. dimension in the direction of the missile axis.
2. Model F-1; a fore-mounted support structure of the same orientation.
3. Model A-3; an aft-mounted model with a 5-in. dimension in the direction of the missile axis.

The grid-point computer input for the three models is given in appendix A.

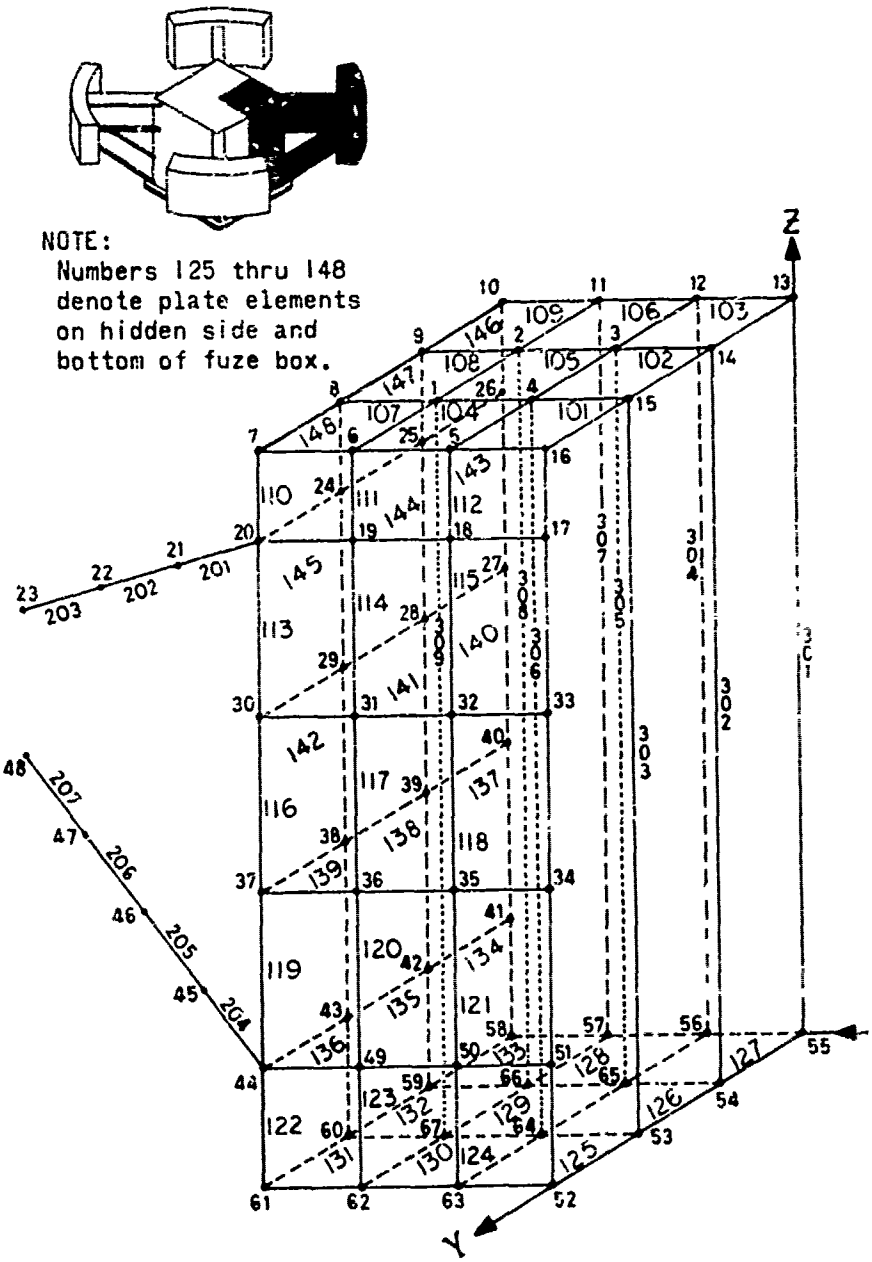

Figure 7. NASTRAN mathematical model for A-1 model.

For models A-1 and F-1, with I-shaped cross sections having the dimensions given in figure 3 (which correspond to the physical dimensions of the experimental models tested), the results for natural frequency given in tables I and II were obtained. The results for natural frequency for model A-3 are given in table III. For model A-3, less material was used in the legs and struts, since they did not need to be as long as in A-1 and F-1. This material savings was utilized to make the flanges of the legs and struts twice as thick as the A-1 and F-1 models (fig. 4).

TABLE I. Natural Frequencies Obtained for Model A-1

MODES	NASTRAN	EXPERIMENTAL
ONE (θ)	-	630
TWO (θ,Z)	722	800
THREE (θ,Z,A)	902	1000

TABLE II. Natural Frequencies Obtained for Model F-1

MODES	NASTRAN	EXPERIMENTAL
ONE (θ)	-	620
TWO (θ,Z)	715	890
THREE (θ,Z,A)	1070	920

TABLE III. Natural Frequencies Obtained for Model A-3

MODES	NASTRAN*
ONE (θ)	-
TWO (θ,Z)	720
THREE (θ,Z,A)	1100

*Values given are those which have the same mode shapes as those for the A-1 and F-1 models.

With this increased cross section, the results obtained for the natural frequencies with the NASTRAN program are given in table II. It should be noted that the normalized deflections and rotations of all grid points, as well as plotted mode shapes, among other things, were obtained as output, but are not presented in this report. An example of the output for A-1 is contained in appendix B.

3. EXPERIMENTAL STUDY

3.1 Model Description

Two models were constructed to check the values of the natural frequencies from the computer for the fore- (F-1) and aft- (A-1) mounted fuze support structures. Figures 1 and 2 show the fore- and aft-mounted fuze structural models.

The fuze box itself was 1/16-in.-thick alodined 6061-T6 aluminum alloy fabricated by bending and welding flat sheet material.

The legs and struts of cross section given in figure 3 were welded to the box; to these were welded the mounting pads shown in figures 5 and 6.

Fuze components were simulated by aluminum blocks of expected size and shape. Figures 8, 9 and 11 give the sizes and arrangement of the individual blocks. This particular arrangement of components gave the center of gravity location shown in figures 10 and 11.

Two Endevco Series 2200 accelerometers were mounted to the simulated component (piece number 11 in fig. 10 and 11) by mounting studs. One was oriented in the negative Z-direction, and the other was oriented in the radial direction aligned with one of the leg axes. (See figure 7 for the coordinate system definition.)

The simulated fuze component assembly was then inserted into the box. Correct standoff distances were maintained by pieces of pre-cast polyurethane foam. The top was attached and 6-lb/ft^3 polyurethane foam was injected through predrilled holes with an approximate 15 percent overfill factor being utilized. The package was cured overnight in an oven at 150°F.

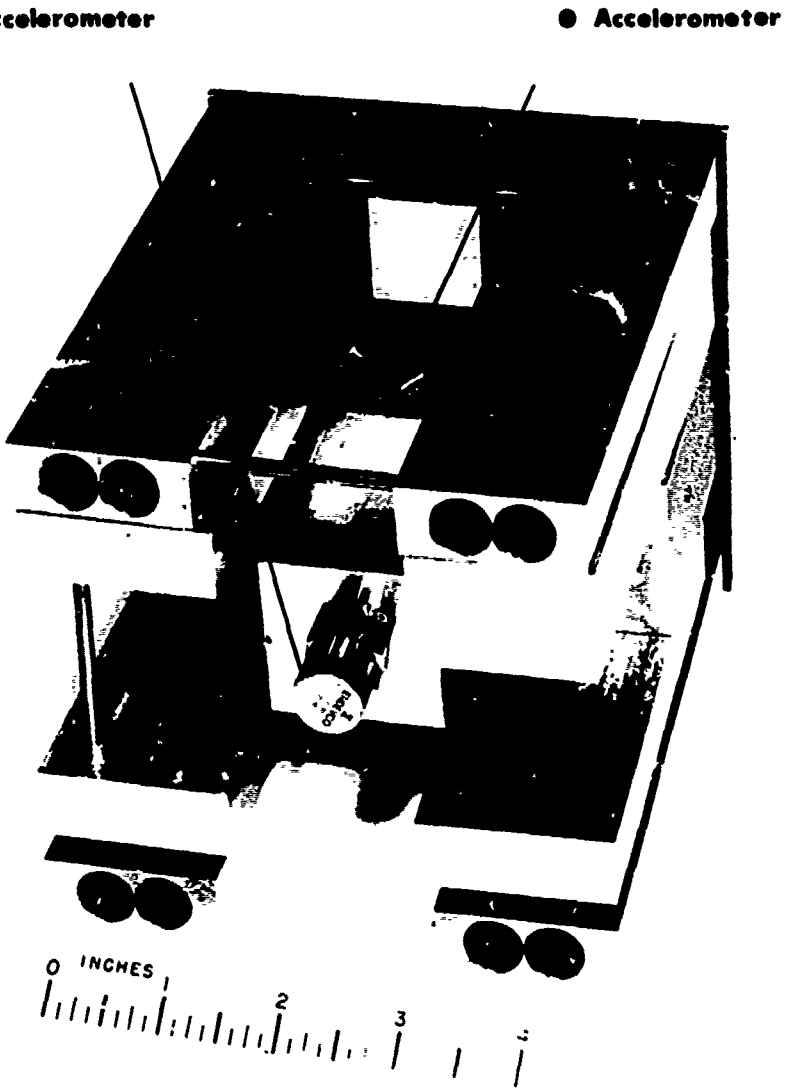

Figure 8. Structural mock-up of fuze components.

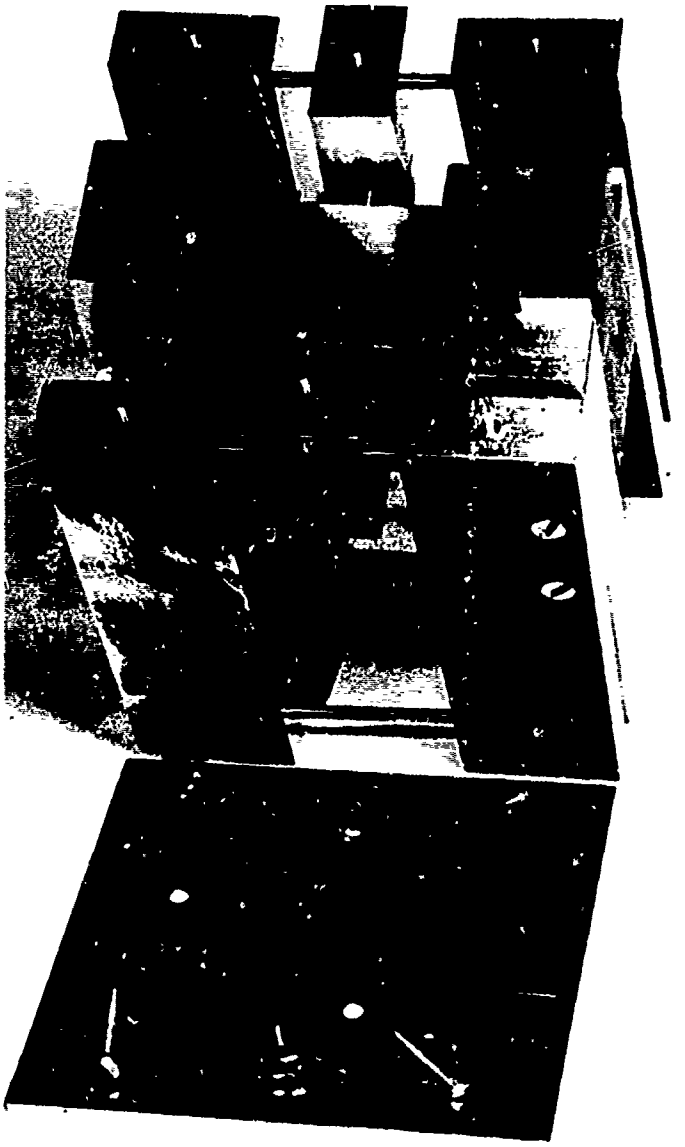

Figure 9. Structural mock-up of fuze components.

After cooling, three additional accelerometers were placed on the outer surface of the fuze package. One was oriented in the negative Z-direction, physically located less than an inch away from the previously mentioned axial accelerometer located on the transmitter block. The second exterior accelerometer was placed on one of the sides of the fuze box and had its axis in the X-Y plane making an angle of 45 deg with the axis of the interior accelerometer oriented in the radial direction. The fifth and final accelerometer on the package was mounted perpendicularly to the web face of one of the struts (in the theta direction) and was used to record rotations of the package about the Z-axis and/or movement of the struts.

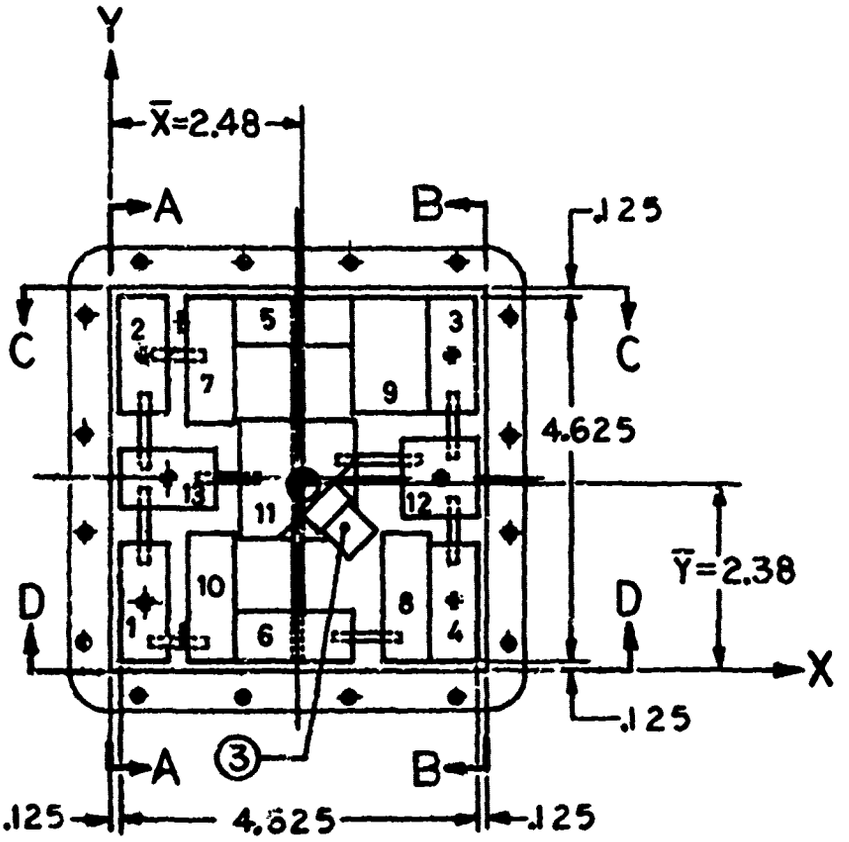

Figure 10. Structural fuze model showing dummy component arrangement, center of gravity, and accelerometers.

Every effort was made to perform identical tests on both A-1 and F-1 units (figs. 12 and 13). The single exception was that the exterior accelerometers on A-1 were Endevco 2200 series, weighing 1.2 oz. each, and those on the F-1 fuze package were Wilcoxon series 102 accelerometers, weighing 0.132 oz. Table IV gives a breakdown for the two units.

TABLE IV. Fuze Mock-up Weight

Box and Top	1.12 lb
Simulated Components	5.92 lb*
Total, A-1	10.12 lb
Total, F-1	10.16 lb

*includes 2 Endevco accelerometers.
Total includes accelerometers and welds.

3.2 A-1 Model Tests

The aft-mounted model was tested by the shock and vibration testing group at HDL on a servo-controlled MB-C25 electrodynamic shaker table and vibra-plane (slip table) system.

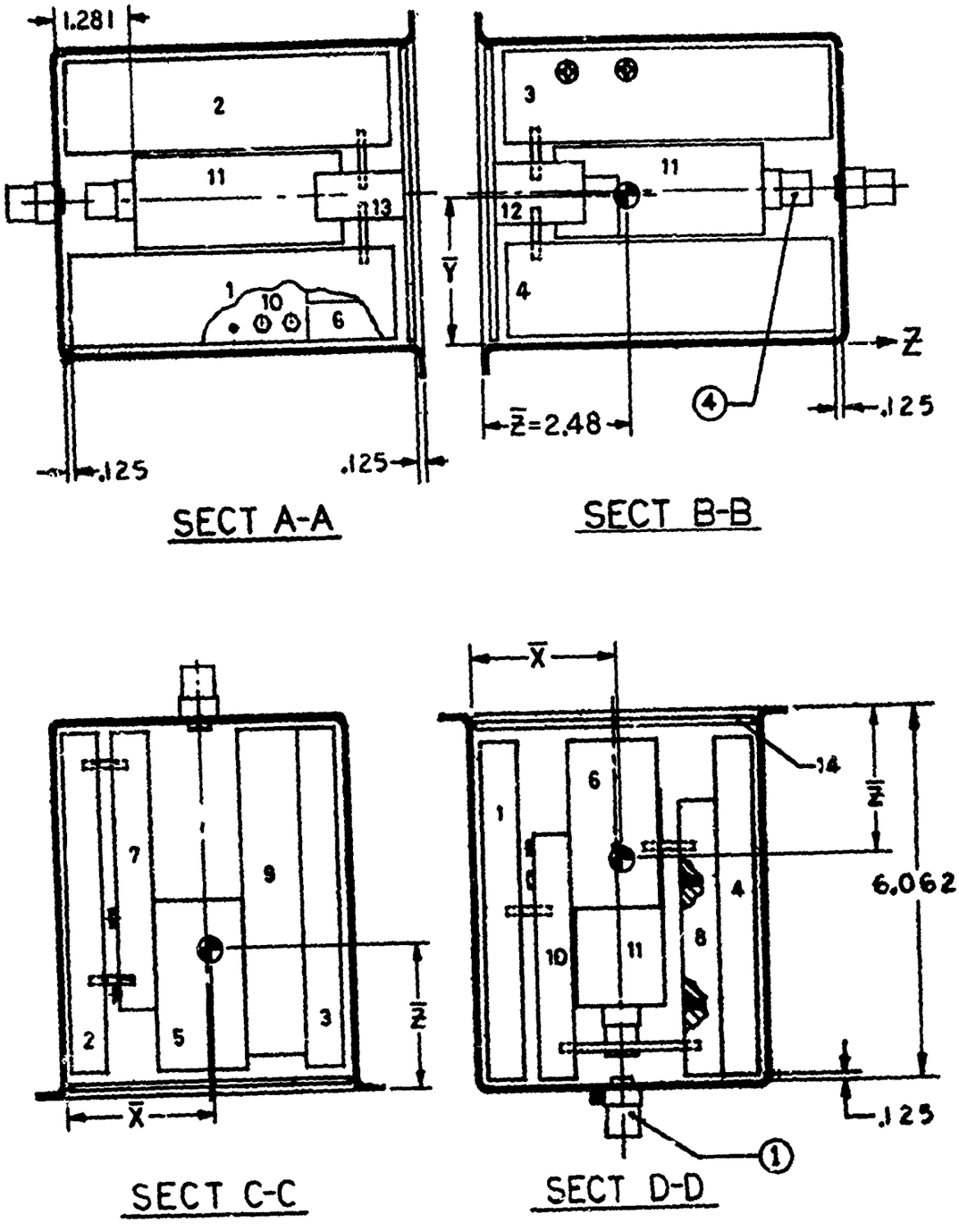

Figure 11. Structural fuze model showing dummy component arrangement, center of gravity, and accelerometers.

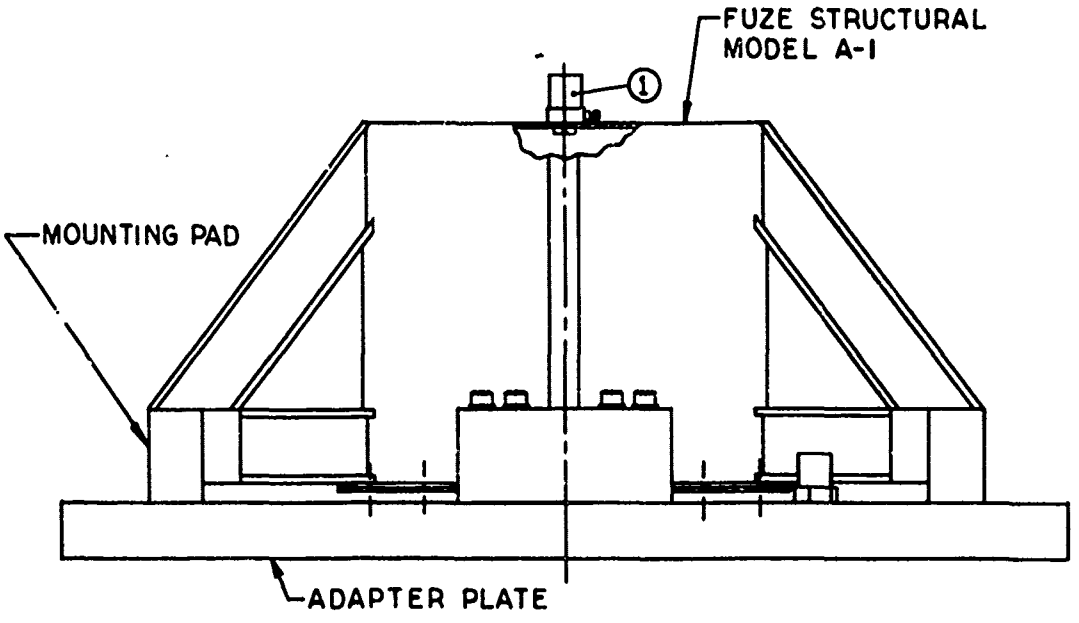

Figure 12. Fuze structural mockup A-1 on shaker adapter plate.

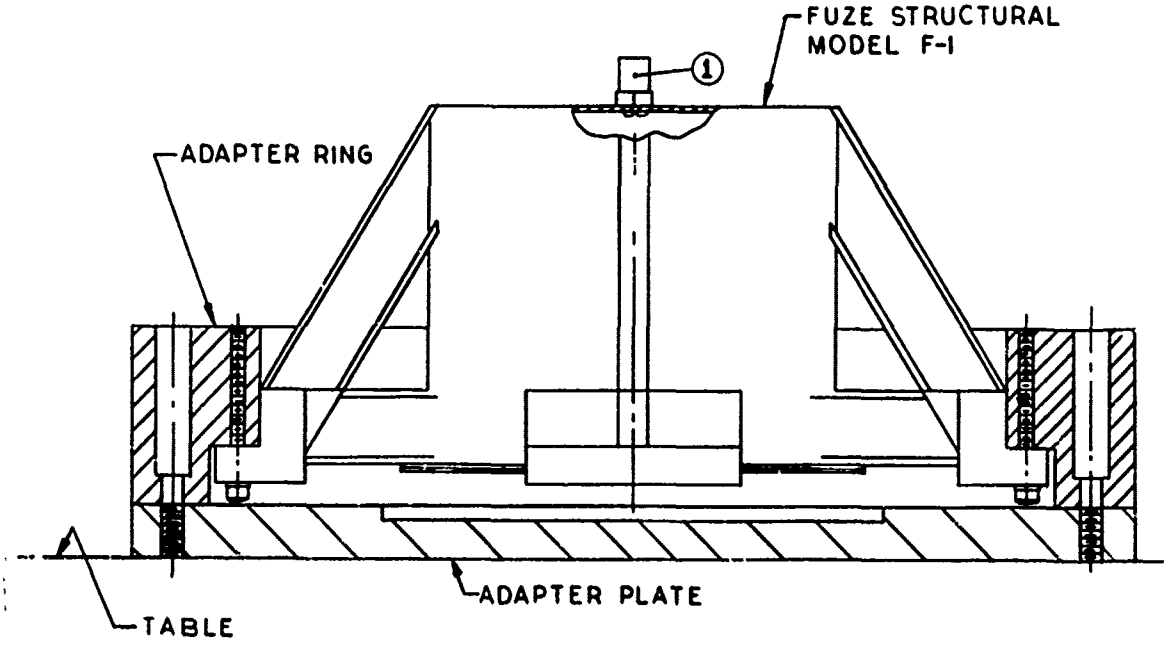

Figure 13. Fuze structural mockup F-1 on shaker adapter plate.

Before testing the fuze package, the adapter plate was attached to the shaker table and tests conducted in both axial and transverse direction to insure that the shaker system had no significant resonances within the range of 20-2000 Hz. The fuze package was then attached to the adapter plate as shown in figure 12 and subjected to sinusoidal vibrations in the Z and X directions at load levels of 2 g with the frequency swept logarithmically from 20 to 2000 and back to 20 Hz in 13 minutes.

Figures 14 and 15 show the fuze structural mock-up being tested in the axial direction. In this direction three runs were conducted at a 2-g load level.

The package was then placed on the slip table and two 2-g vibration tests were conducted with the sinusoidal force being applied in the X direction (fig. 16).

Good shaker amplitude control was achieved in the first 2-g run in the axial direction. However, normal amplitude tolerance (±10 percent) was exceeded severalfold over two narrow, closely spaced frequency bands in all other tests. These data were therefore less reliable.

3.3 F-1 Model Tests

The fore-mounted model was tested on an MB-C150 shaker and slip table system by General Testing Laboratories (GTL) at their site in Hartwood, Virginia.

A special adapter ring was required to simulate the forward mounting condition. A drawing of the package attached to this ring and an adapter plate is shown in figure 13. As before, axial and transverse tests were conducted on the adapter ring, adapter plate, and shaker alone to determine their response in the range of frequencies of interest.

The package was then bolted to the adapter ring and sinusoidal 2-g loads were applied in the axial (Z) and two transverse directions (X and 45 deg from the X directions). Once again the frequency range from 20 to 2000 and back to 20 Hz was swept in 13 minutes. Shaker Shaker control throughout the entire test program at GTL was excellent, and the data obtained were complete.

4. RESULTS

The data obtained from the tests are presented in figures 17 through 25, where amplification (recorded g-level divided by table input g-level) versus frequency is plotted for each of the five accelerometer locations in each of the three different directions of loading. The results obtained from the fore- and aft-mounted models were both plotted on the same figure for direct comparison.

For the A-1 model the natural frequencies are seen to occur at 630, 800, 1000, and 1600 Hz. The resonance at 630 Hz was observed only as a rotation about the Z-axis with no other accelerometer showing any increase in amplification at this frequency. The 800-Hz mode is excited only under transverse loading conditions with the 1000-Hz mode being present in the data obtained from both the axial and transverse vibrations. The 1600-Hz resonance was evident only on exterior-mounted accelerometers and not on those that were placed on the simulated fuze components. For the F-1 model, the natural frequencies occurred near 620, 890, 920, and 1650 Hz. Once again, the 620-Hz value was due to a rotation

only. The 890- and 1650-Hz values were obtained from transverse excitations only, and the 920-Hz mode was the only mode excited during axial vibration. These values of natural frequencies are summarized in table V.

TABLE V. Experimentally Obtained Natural Frequencies (Hz)

A-1	630	800	1000	1600
F-1	620	890	920	1650

Tables I and II show that it was possible to match resonant frequencies obtained experimentally with a frequency and mode shape obtained using NASTRAN. This correspondence was not complete, however, as NASTRAN produced more frequencies in the range 20-2000 Hz than were found in the vibration experiment (app. B). At least some of the additional natural frequencies obtained by NASTRAN can be discounted, because the mode shapes indicated movement in places that would not have been detected by the accelerometers used in the experiments. In addition, no information was available from the normal mode analysis, which indicated the amplification factor for each natural frequency. Thus, the possibility exists that some of the frequencies obtained by NASTRAN were of too small an order to be detected by the experimental equipment. Finally, an improved mathematical NASTRAN model would most likely eliminate some of those frequencies that cannot be discounted according to the reasoning explained above. This would also correct the failure of the NASTRAN solutions to correspond to the frequencies detected by the accelerometer mounted on one of the struts.

5. CONCLUSIONS

Figures 17 through 25, which are discrete point plots selected from continuous recorder traces, provide the basis for some conclusions.

Figures 17 and 22, which show the response of an accelerometer attached to a fuze package support strut, give evidence that the lowest natural frequency for both models A-1 and F-1 occurred at about 630 Hz in a rotational mode about the Z-axis. This mode was excited when the vibration inputs to the models were in either axial or transverse directions.

The next natural frequencies of large amplification occurred at about 800 Hz and near 1000 Hz, measured on the box surface. These coincided with two of the NASTRAN modes (Table I).

The lowest frequencies excited by axial vibration were 900 Hz for the fore-mounted model and 820 Hz for the aft-mounted model, measured inside the box (fig. 19). No comparison with a NASTRAN prediction was possible since the mathematical model did not include internal grid points.

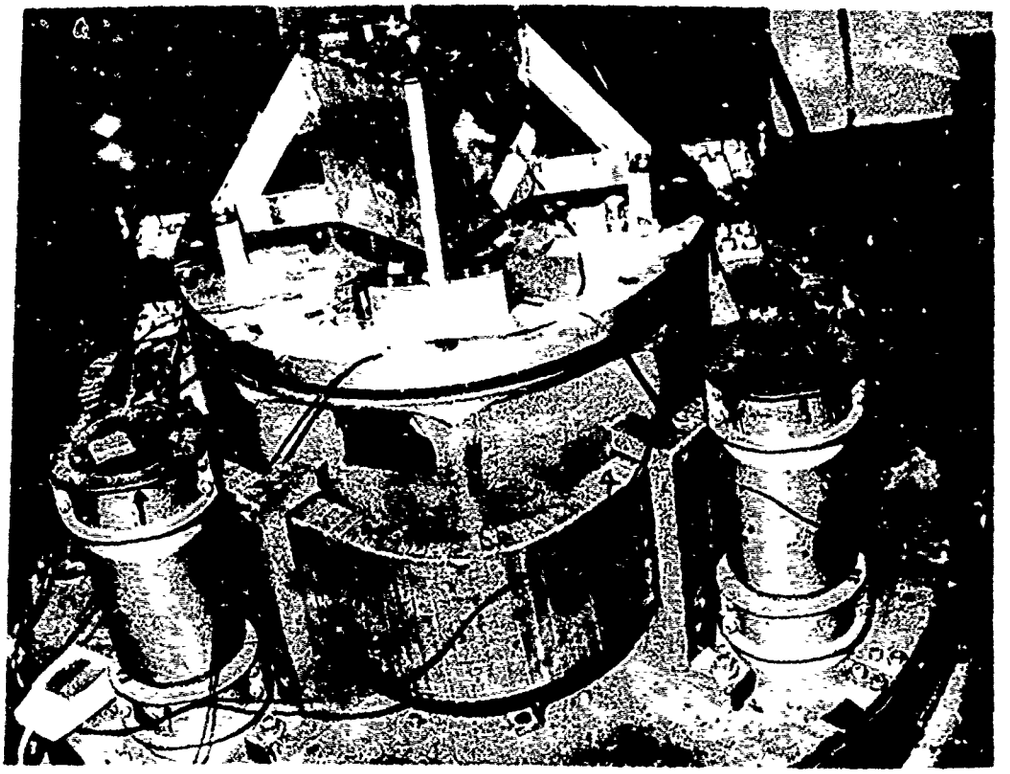

Figure 14. Fuze structural mockup A-1 ready for vibration test.

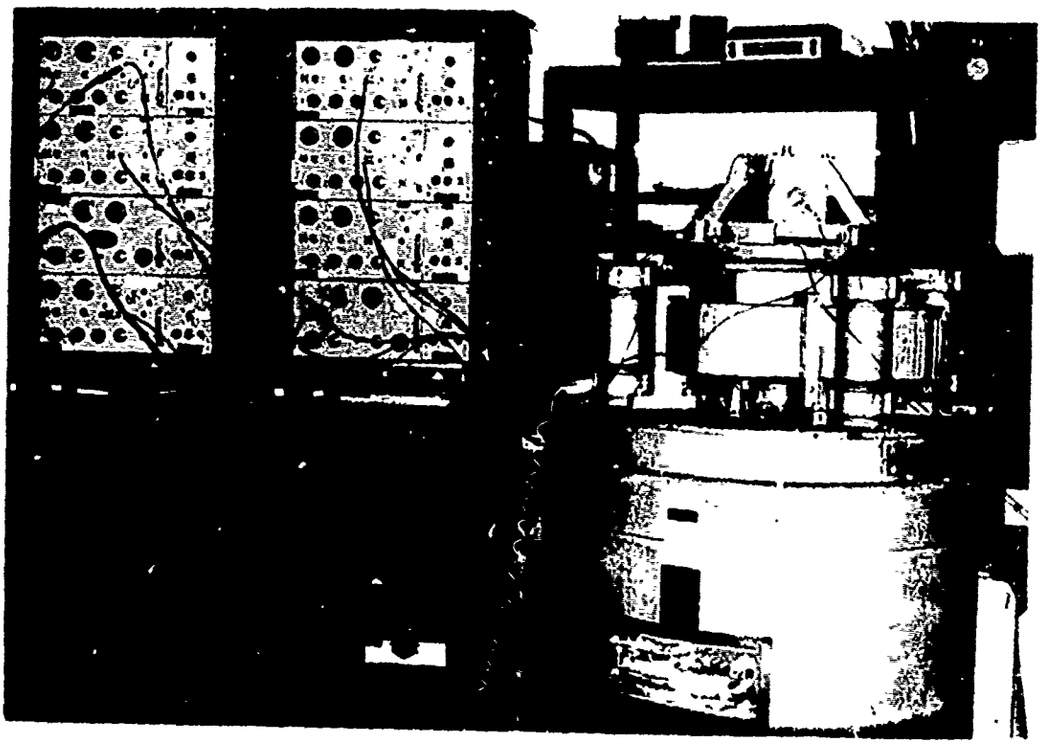

Figure 15. Vibration test setup for Z-axis exitation of A-1 fuze mockup.

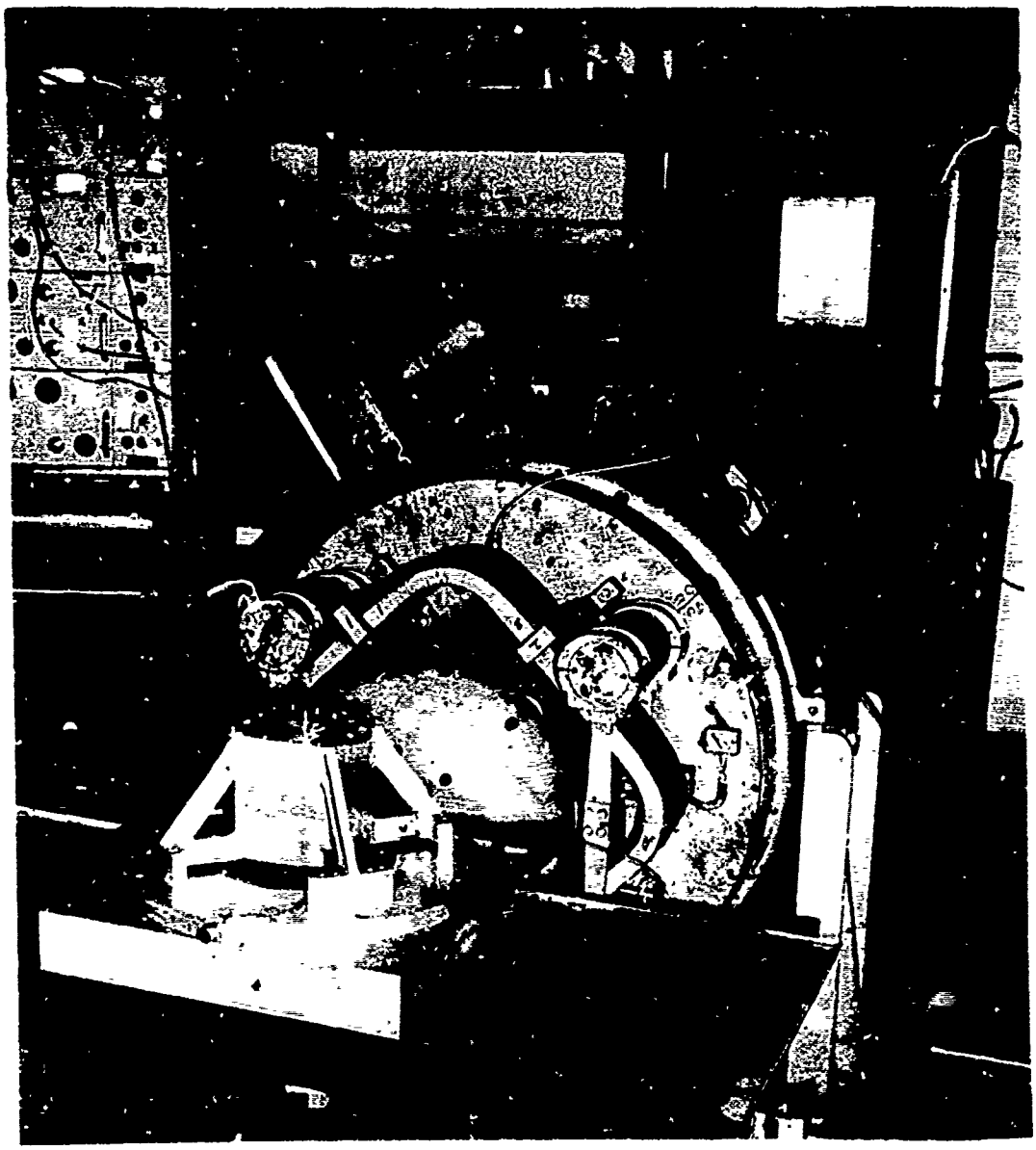

Figure 16. Vibration test setup for transverse exitation of A-1 fuze mockup.

6. RECOMMENDATIONS

The proposed fuze structure design study should be continued in the following ways:

First, since a better picture now exists of the actual fuze size, geometry, and orientation, this information should be used as input to the NASTRAN program. This input should utilize the previously mentioned formats. The structure should then be examined under sinusoidal loading at or near predicted natural frequencies to determine damage potential of resonant loading.

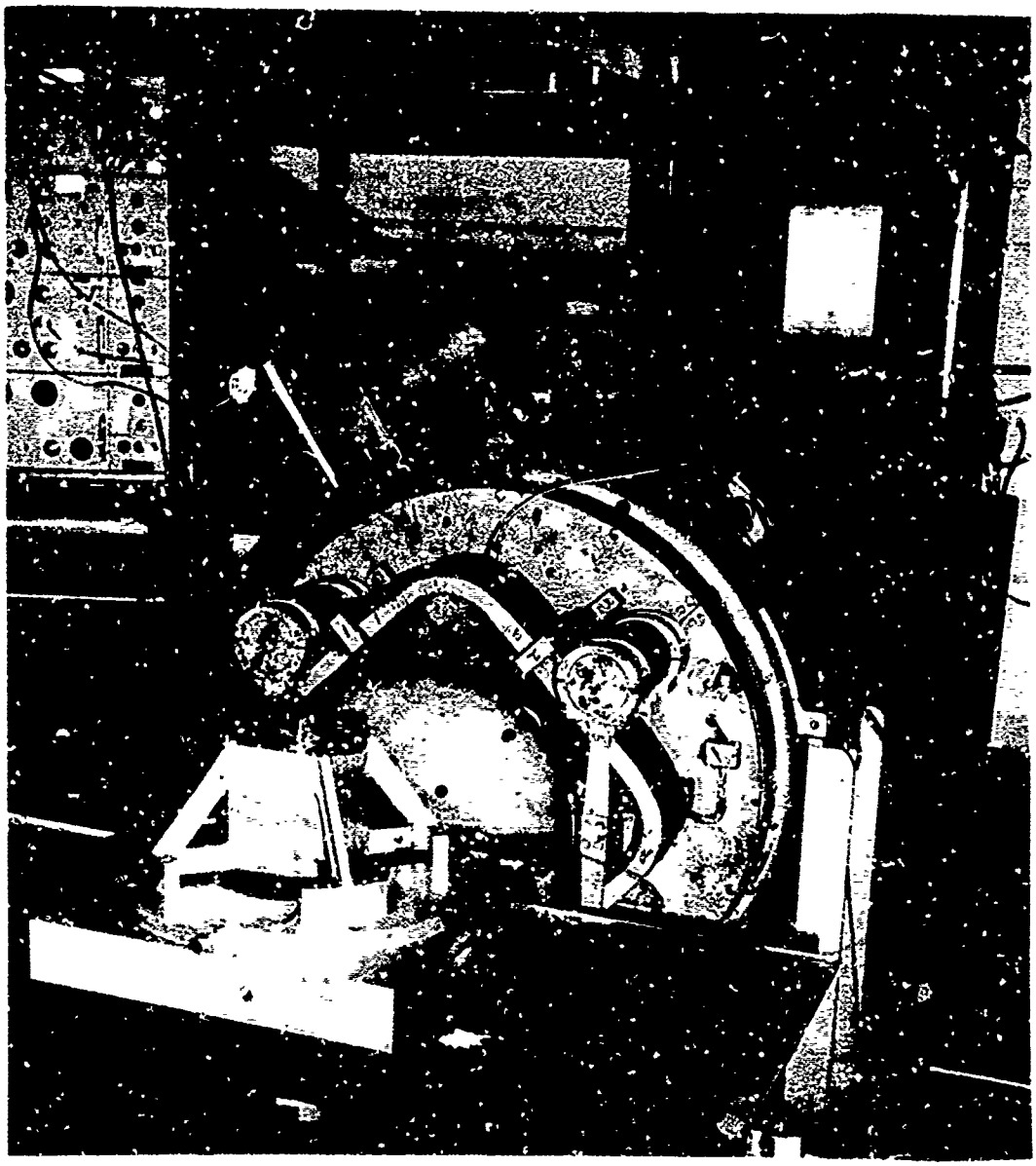

Figure 1 Vibration test setup for transverse exitation of A-1 fuze mockup.

6. RECOMMENDATIONS

The proposed fuze structure design study should be continued in the following ways:

First, since a better picture now exists of the actual fuze size, geometry, and orientation, this information should be used as input to the NASTRAN program. This input should utilize the previously mentioned formats. The structure should then be examined under sinusoidal loading at or near predicted natural frequencies to determine damage potential of resonant loading.

An improved mathematical model should be employed that utilizes more grid points and more realistically represents the polyurethane foam in the X and Y directions. (Such a model is in progress and will be reported in Part II of this study.)

It appears that the lowest resonant mode obtained for the proposed fuze structure was sufficiently high for component survival. The second natural frequency, which was excited by transverse vibration (800 Hz for A-1 and 890 Hz for F-1), was of a more serious nature. Therefore, some consideration might be given to increase these frequencies as well as those that occurred in the axial mode of vibration. The lowest natural frequency of the axial mode can be raised by increasing the moments of inertia of the legs and struts; this can be done within specified weight limitations. This weight addition, however, also adds to the supported weight, and there are indications (from other NASTRAN runs performed but not reported here) that this tends to lower slightly the natural frequencies excited by transverse vibration. The suggestion, therefore is that the NASTRAN program be utilized to its full potential, and such things as tapered, laminated, and unsymmetrical beam sections be investigated, if these natural frequencies are to be increased.

The assumption was made that the mounting pads gave absolute fixity to the ends of the legs and struts. This, in reality, is not true, because the ring on which these pads are mounted moves due to elasticity of the missile itself. It is recommended that by the use of scalar points and connecting linear springs, the NASTRAN program be used to determine the natural frequencies as a function of missile elasticity.

Finally, it was noted that there was a small decrease in the natural frequencies when the original dip-brazed structure was welded. If possible, a mock-up of the proper size, orientation, and mounting pad type, manufactured by a casting process should be tested and compared with NASTRAN results obtained for a similar welded structure.

ACKNOWLEDGEMENTS

The authors wish to thank HDL contributors H. Murphy, P. McWortel, G. Blevins, and J. Simpson for model fabrication, R. Glaser for help in vibration tests, and M. Mandzak for drafting. Many helpful consultations were provided by J. McKee of NSRDC and G.J. Hutchins of HDL.

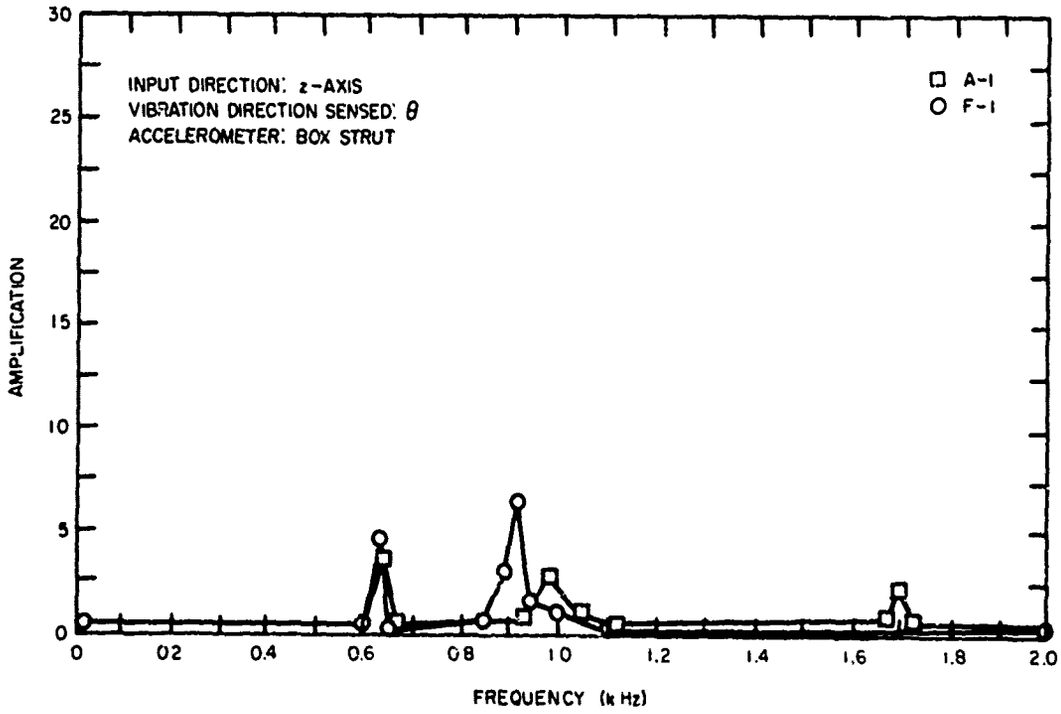

Figure 17. Response of models A-1 and F-1 to 2-g sinusoidal input.

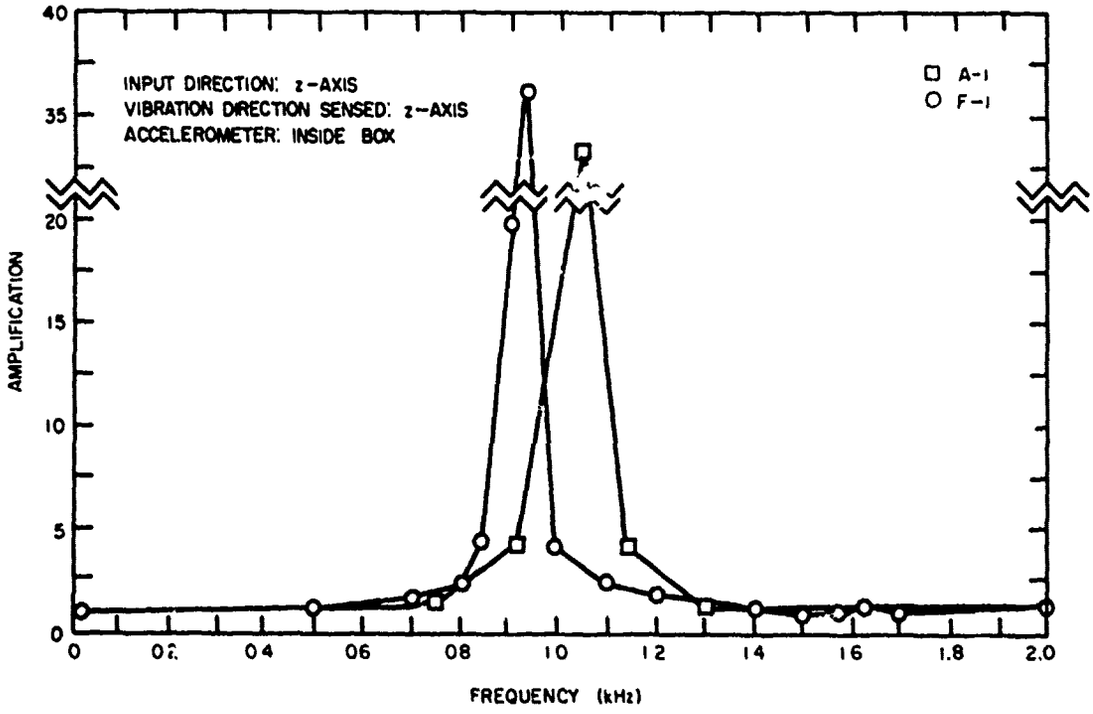

Figure 18. Response of models A-1 and F-1 to 2-g sinusoidal input.

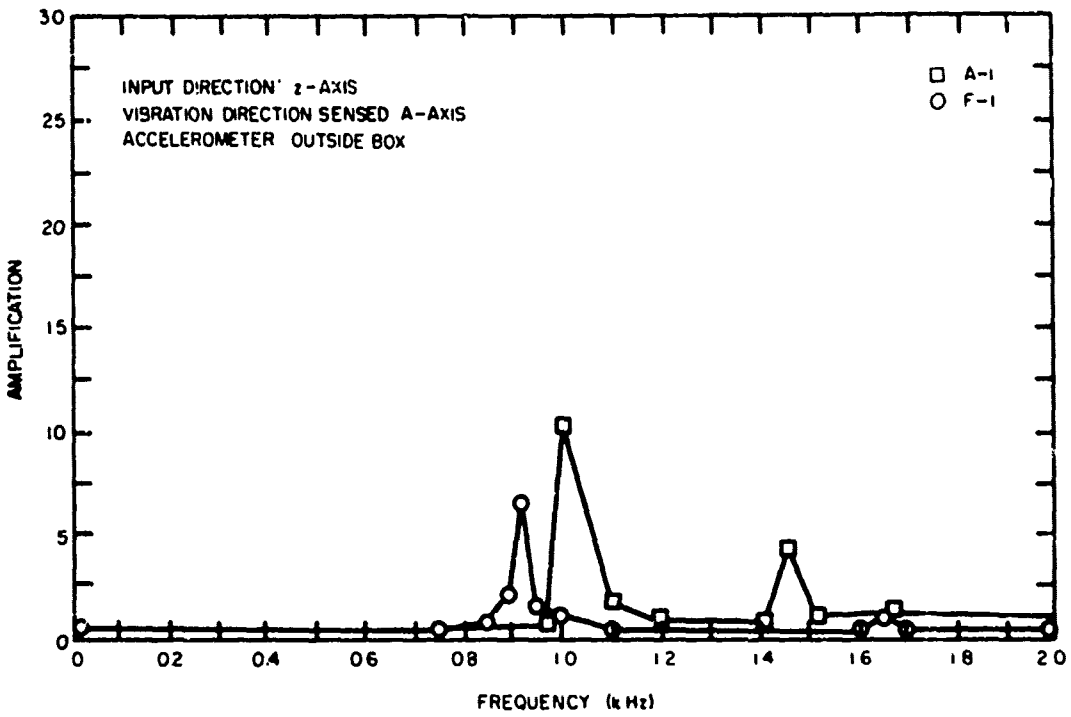

Figure 19. Response of models A-1 and F-1 to 2-g sinusoidal input.

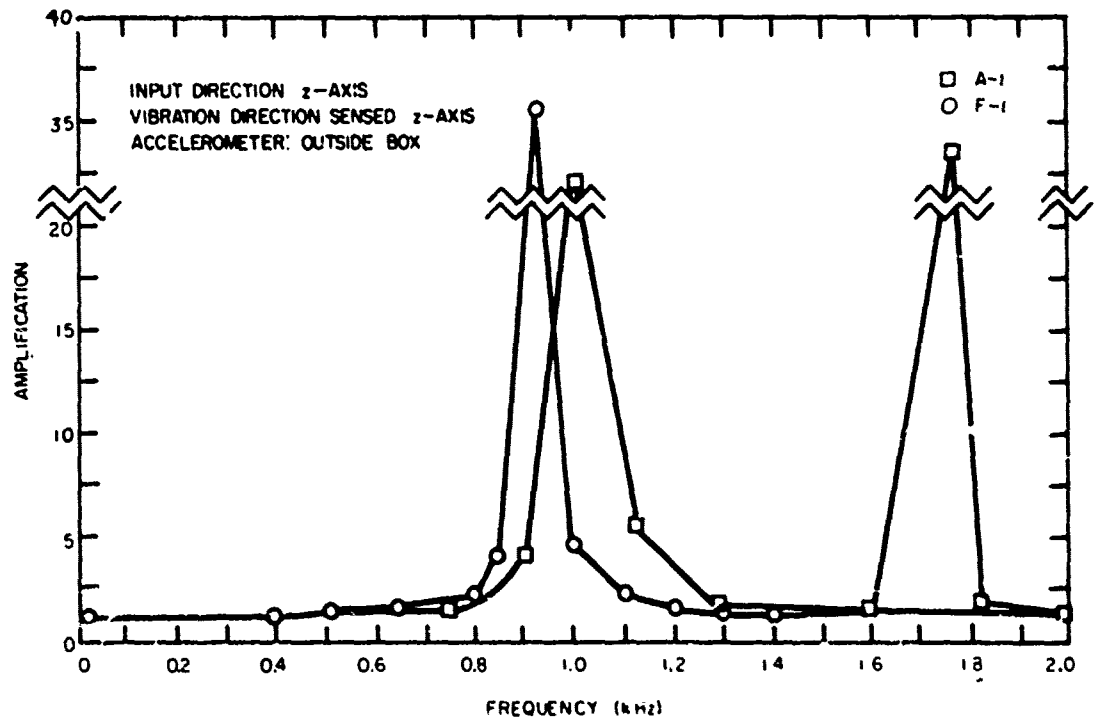

Figure 20. Response of models A-1 and F-1 to 2-g sinusoidal input.

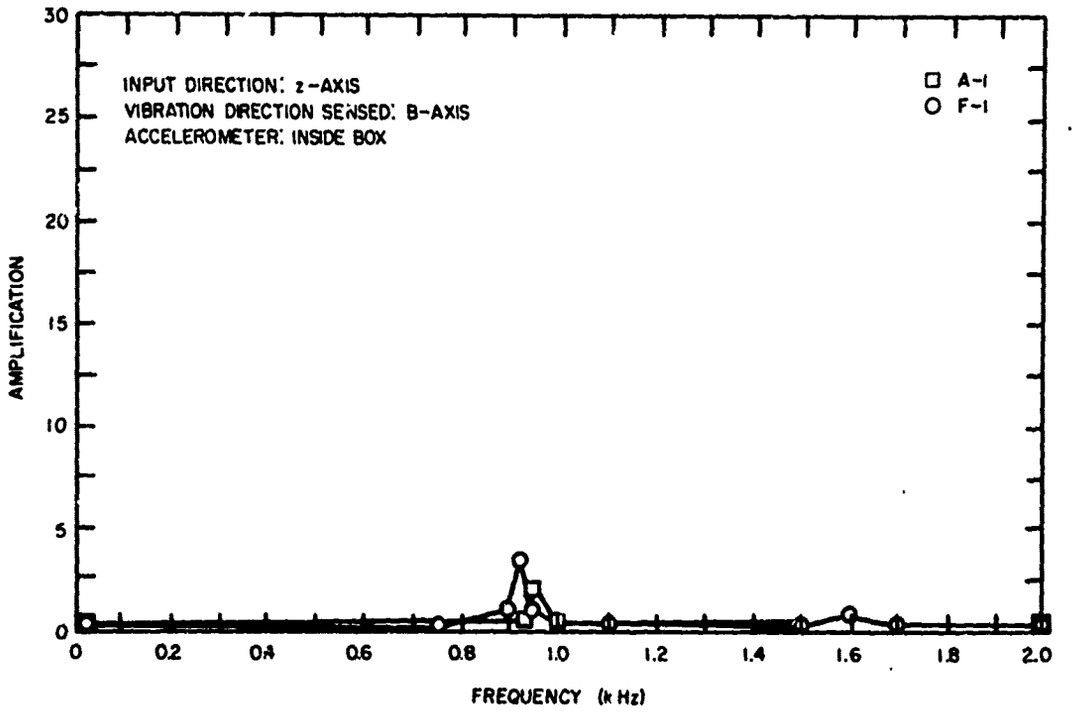

Figure 21. Response of models A-1 and F-1 to 2-g sinusoidal input.

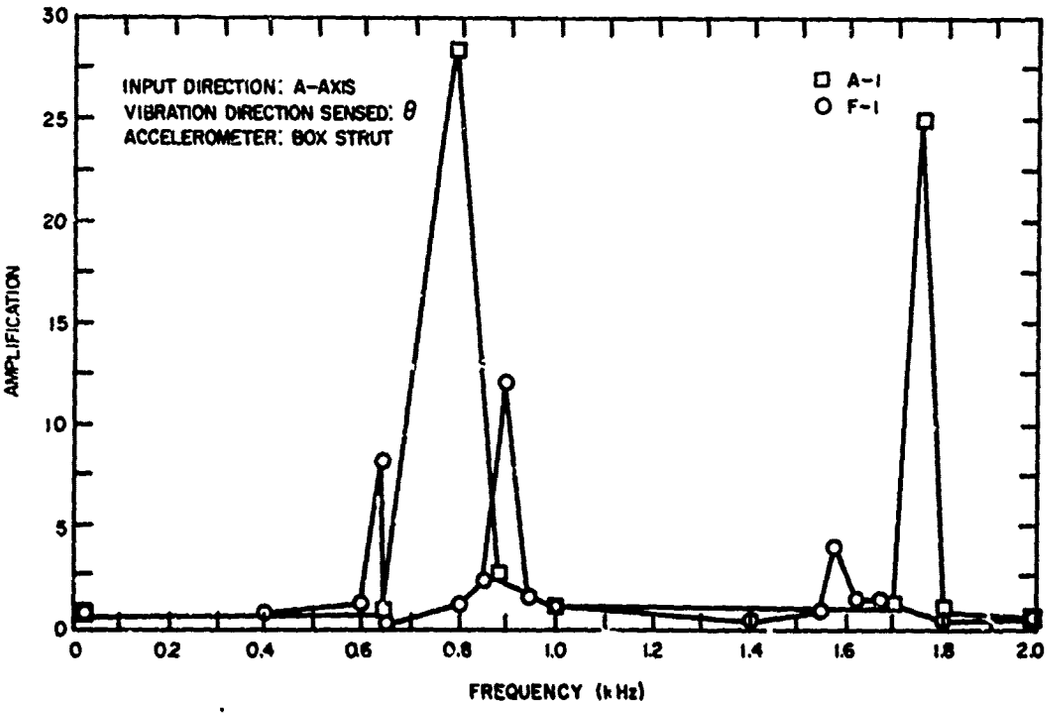

Figure 22. Response of models A-1 and F-1 to 2-g sinusoidal input.

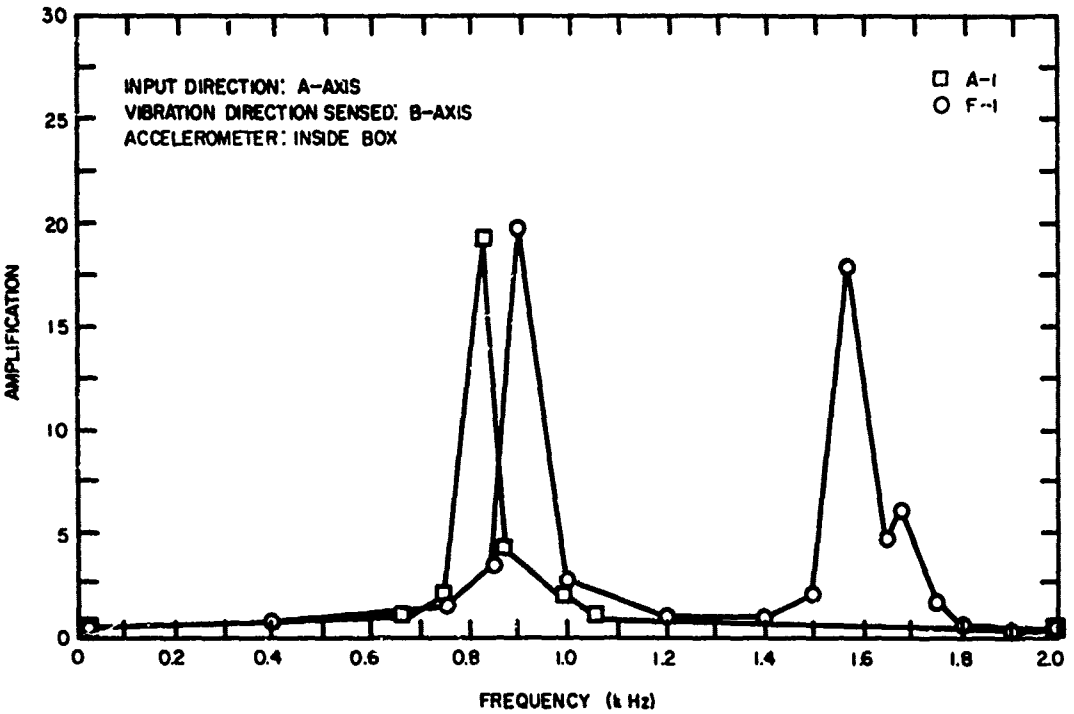

Figure 23. Response of models A-1 and F-1 to 2-g sinusoidal input.

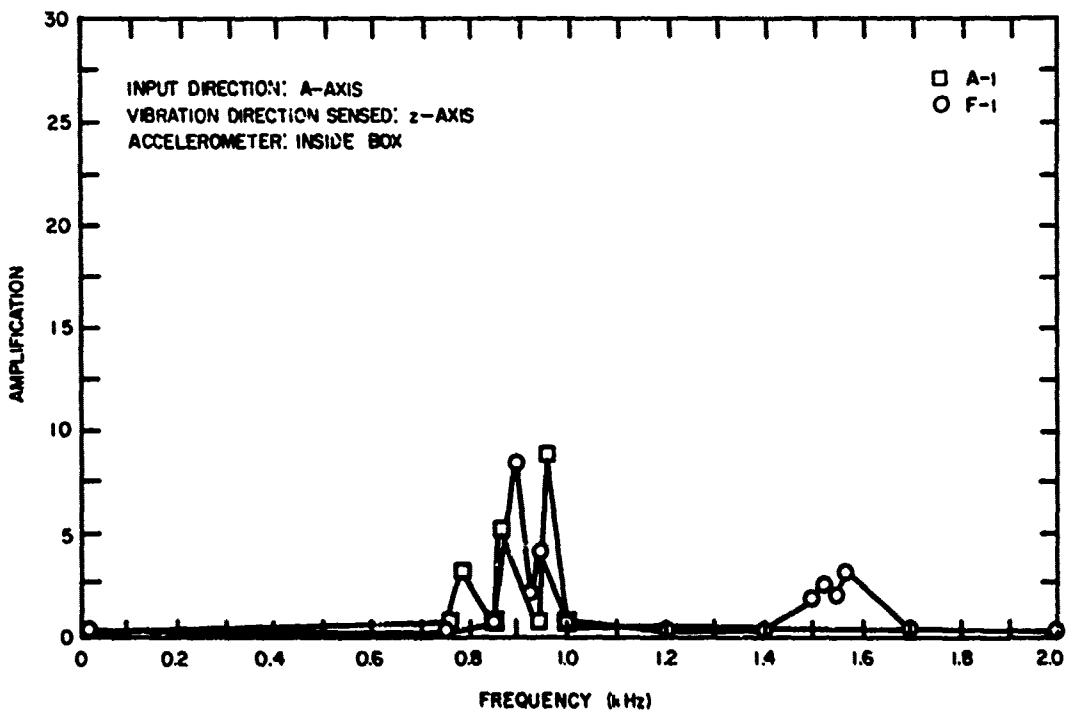

Figure 24. Response of models A-1 and F-1 to 2-g sinusoidal input.

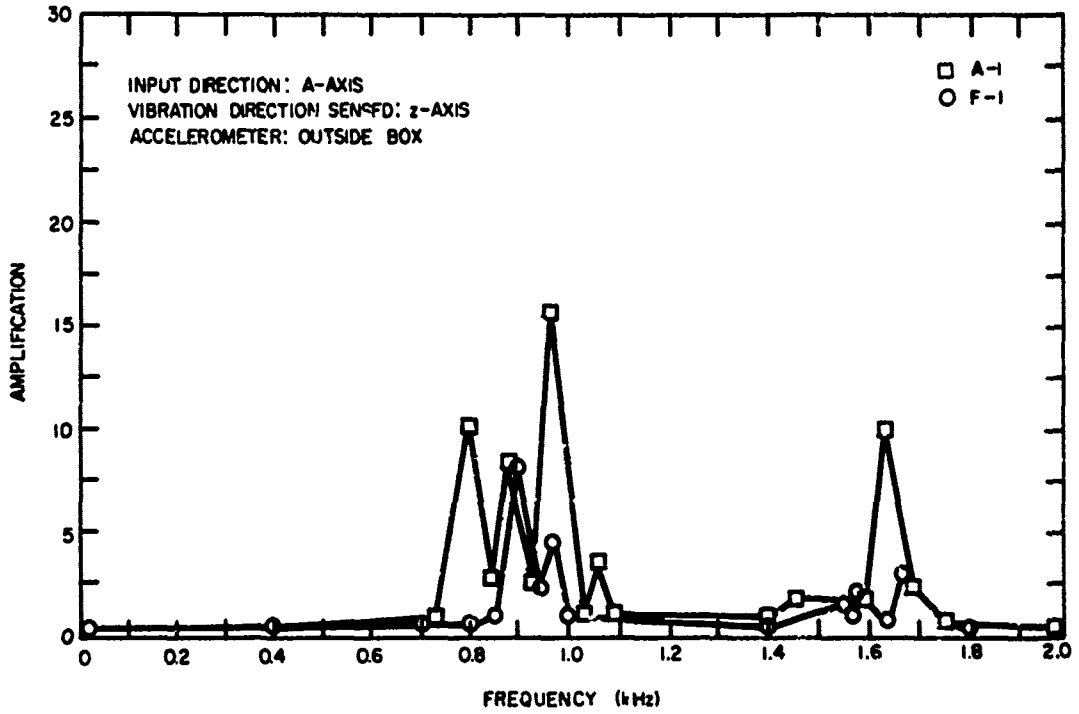

Figure 25. Response of models A-1 and F-1 to 2-g sinusoidal input.

APPENDIX A. INPUT DATA TO NASTRAN FOR FUZE MODEL A-1

SORTED BULK DATA ECHO

CARD COUNT	1	2	3	4	5	6	7	8	9	10
1	CBAR	201	20	20	21	1.0	1.0	1.0	1	
2	CBAR	202	20	21	22	1.0	1.0	1.0	1	
3	CBAR	203	20	22	23	1.0	1.0	1.0	1	
4	CBAR	204	21	44	45	1.0	1.0	6.0	1	
5	CBAR	205	21	45	46	1.0	1.0	6.0	1	
6	CBAR	206	21	46	47	1.0	1.0	6.0	1	
7	CBAR	207	21	47	48	1.0	1.0	6.0	1	
8	CORD2C	2	1	.0	.0	.0	.0	.0	1.0	134
9	634	1.0	0.0	1.0						
10	CORD2R	1	0	.0	.0	.0	.0	.0	1.0	123
11	623	1.0	0.0	1.0						
12	CQUAD2	101	22	5	16	15	4	.0		
13	CQUAD2	102	22	4	15	14	3	.0		
14	CQUAD2	103	22	3	14	13	12	.0		
15	CQUAD2	104	22	6	5	4	1	.0		
16	CQUAD2	105	22	1	4	3	2	.0		
17	CQUAD2	106	22	2	3	12	11	.0		
18	CQUAD2	107	22	7	6	1	8	.0		
19	CQUAD2	108	22	8	1	2	9	.0		
20	CQUAD2	109	22	9	2	11	10	.0		
21	CQUAD2	110	25	20	19	6	7	.0		
22	CQUAD2	111	25	19	18	5	6	.0		
23	CQUAD2	112	25	18	17	16	5	.0		
24	CQUAD2	113	25	30	31	19	20	.0		
25	CQUAD2	114	25	31	32	18	19	.0		
26	CQUAD2	115	25	32	33	17	18	.0		
27	CQUAD2	116	25	37	36	31	30	.0		
28	CQUAD2	117	25	36	35	32	31	.0		
29	CQUAD2	118	25	35	34	33	32	.0		
30	CQUAD2	119	25	44	49	36	37	.0		
31	CQUAD2	120	25	49	50	35	36	.0		
32	CQUAD2	121	25	50	51	34	35	.0		
33	CQUAD2	122	25	61	62	49	44	.0		
34	CQUAD2	123	25	62	63	50	49	.0		
35	CQUAD2	124	25	63	52	51	50	.0		
36	CQUAD2	125	22	63	64	53	52	.0		
37	CQUAD2	126	22	64	65	54	53	.0		
38	CQUAD2	127	22	65	56	55	54	.0		
39	CQUAD2	128	22	66	57	56	65	.0		
40	CQUAD2	129	22	67	66	65	64	.0		
41	CQUAD2	130	22	62	67	64	63	.0		
42	CQUAD2	131	22	61	60	67	62	.0		
43	CQUAD2	132	22	60	59	66	67	.0		
44	CQUAD2	133	22	59	58	57	66	.0		
45	CQUAD2	134	25	59	42	41	58	.0		
46	CQUAD2	135	25	60	43	42	59	.0		
47	CQUAD2	136	25	61	44	43	60	.0		
48	CQUAD2	137	25	42	39	40	41	.0		
49	CQUAD2	138	25	43	38	39	42	.0		
50	CQUAD2	139	25	44	37	38	43	.0		
51	CQUAD2	140	25	39	28	27	40	.0		
52	CQUAD2	141	25	38	29	28	39	.0		
53	CQUAD2	142	25	37	30	29	38	.0		
54	CQUAD2	143	25	28	25	26	27	.0		
55	CQUAD2	144	25	29	24	25	28	.0		
56	CQUAD2	145	25	30	20	24	29	.0		
57	CQUAD2	146	25	25	9	10	26	.0		
58	CQUAD2	147	25	24	8	9	25	.0		
59	CQUAD2	148	25	20	7	8	24	.0		
60	CROD	301	23	55	13					
61	CROD	302	23	54	14					
62	CROD	303	23	53	15					
63	CROD	304	23	56	12					
64	CROD	305	23	55	3					
65	CROD	306	23	64	4					
66	CROD	307	23	57	11					
67	CROD	308	23	66	2					
68	CROD	309	23	67	1					
69	EIGR	1	GIV	.0	2000.0		10			&ABD
70	&ABD	MAX								
71	SPCSET		1				1			
72	GRID	1		1.667	1.667	6.0				
73	GRID	2		1.667	.833	6.0				
74	GRID	3		.833	.833	6.0				
75	GRID	4		.833	1.667	6.0				

```
76      GRID    5                       .833    2.5     6.0
77      GRID    6                       1.667   2.5     6.0
78      GRID    7                       2.5     2.5     6.0
79      GRID    8                       2.5     1.667   6.0
80      GRID    9                       2.5     .833    6.0
81      GRID    10                      2.5     .0      6.0
82      GRID    11                      1.667   .0      6.0
83      GRID    12                      .833    .0      6.0
84      GRID    13                      .0      .0      6.0
85      GRID    14                      .0      .833    6.0
86      GRID    15                      .0      1.667   6.0
87      GRID    16                      .0      2.5     6.0
88      GRID    17                      .0      2.5     5.375
89      GRID    18                      .833    2.5     5.375
90      GRID    19                      1.667   2.5     5.375
91      GRID    20                      2.5     2.5     5.375
92      GRID    21      2               4.25    45.     5.375
93      GRID    22      2               4.96    45.     5.375   123456
94      GRID    23      2               5.67    45.     5.375
95      GRID    24                      2.5     1.667   5.375
96      GRID    25                      2.5     .833    5.375
97      GRID    26                      2.5     .0      5.375
98      GRID    27                      2.5     .0      3.922
99      GRID    28                      2.5     .833    3.922
100     GRID    29                      2.5     1.667   3.922
101     GRID    30                      2.5     2.5     3.922
102     GRID    31                      1.667   2.5     3.922
103     GRID    32                      .833    2.5     3.922
104     GRID    33                      .0      2.5     3.922
105     GRID    34                      .0      2.5     2.468
106     GRID    35                      .833    2.5     2.468
107     GRID    36                      1.667   2.5     2.468
108     GRID    37                      2.5     2.5     2.468
109     GRID    38                      2.5     1.667   2.468
110     GRID    39                      2.5     .833    2.468
111     GRID    40                      2.5     .0      2.468
112     GRID    41                      2.5     .0      1.015
113     GRID    42                      2.5     .833    1.015
114     GRID    43                      2.5     1.667   1.015
115     GRID    44                      2.5     2.5     1.015
116     GRID    45      2               4.27    45.     1.949
117     GRID    46      2               5.00    45.     2.883
118     GRID    47      2               5.73    45.     3.817
119     GRID    48      2               6.46    45.     4.750   123456
120     GRID    49                      1.667   2.5     1.015
121     GRID    50                      .833    2.5     1.015
122     GRID    51                      .0      2.5     1.015
123     GRID    52                      .0      2.5     .0
124     GRID    53                      .0      1.667   .0
125     GRID    54                      .0      .833    .0
126     GRID    55                      .0      .0      .0
127     GRID    56                      .833    .0      .0
128     GRID    57                      1.667   .0      .0
129     GRID    58                      2.5     .0      .0
130     GRID    59                      2.5     .833    .0
131     GRID    60                      2.5     1.667   .0
132     GRID    61                      2.5     2.5     .0
133     GRID    62                      1.667   2.5     .0
134     GRID    63                      .833    2.5     .0
135     GRID    64                      .833    1.667   .0
136     GRID    65                      .835    .833    .0
137     GRID    66                      1.667   .833    .0
138     GRID    67                      1.667   1.667   .0
139     MAT1    30      10.066                  .3      2.54-4
140     MAT1    31      10.066                  .3      2.54-4
141     MAT1    32      10.066                  .3      2.54-4
142     MAT1    33      4.9663  1.363                   8.97-6
143     OMIT1   4       14      15      16      17      33      34      51      &MFT
144     &MFT    52      53      54      27      26      10      11      12      &MET
145     OMIT1   5       41      40      58      57      64      65      66      &MAT
146     &MET    56      1       2       3       4       67      35      49      &MBT
147     OMIT1   45      19      18      31      32      36      29      28      24      &MIT
148     &MAT    67      42      43      39      38      56      21      22      &567
149     OMIT1   46      5       6       7       8       9       44      59      &678
150     &MBT    50      30      37      45      46      47
151     OMIT1   56      20      61      62      63
152     &MIT    25      60
153     OMIT1   456
154     &567    20
155     &678    60
156     PARAM   GRDPNT  100
```

```
157     PBAR    20      30      .25     2.76-3  5.-2    1.3-3
158     PBAR    21      31      .25     2.76-3  5.-2    1.3-3
159     PQUAD2  22      32      6.25-2  1.56-4
160     PQUAL2  25      32      6.25-2  6.46-5
161     PROD    23      33      1.0     .0
162     SEQGP   1       13      2       12      3       5       4       10
163     SEQGP   5       20      6       21      7       25      8       24
164     SEQGP   9       23      10      22      11      11      12      4
165     SEQGP   13      1       14      3       15      9       16      19
166     SEQGP   17      35      18      36      19      37      20      38
167     SEQGP   21      53      22      63      23      65      24      41
168     SEQGP   25      40      26      39      27      55      28      56
169     SEQGP   29      54      30      52      31      51      32      50
170     SEQGP   33      49      34      61      35      45      36      47
171     SEQGP   37      60      38      59      39      58      40      57
172     SEQGP   41      42      42      43      43      44      44      48
173     SEQGP   45      62      46      64      47      66      48      67
174     SEQGP   49      46      50      29      51      28      52      31
175     SEQGP   53      16      54      7       55      2       56      6
176     SEQGP   57      14      58      27      59      28      60      30
177     SEQGP   61      34      62      33      63      32      64      17
178     SEQGP   65      8
179     SEQGP   66      15
180     SEQGP   67      18
181     SPC1    10      4       41      42      43      40      37      38      &SPC11
182     &SPC11  39      26      29      28      27      24      25
183     SPC1    10      5       19      18      17      31      32      33      &SPC12
184     &SPC12  36      35      34      49      50      51
185     SPC1    10      6       1       2       11      12      13      3       &SPC13
186     &SPC13  14      4       55      56      57      54      65      66      &SPC14
187     &SPC14  63      64      67      15
188     SPC1    10      196     13      14      15      16      17      33      &SPC15
189     &SPC15  34      51      52      53      54      55
190     SPC1    10      246     13      12      11      10      26      27      &SPC16
191     &SPC16  40      41      58      57      56      55
        ENDLATA
```

APPENDIX B. SAMPLE OF NASTRAN OUTPUT FOR FUZE MODEL A-1.

REAL EIGENVALUES

MODE NO.	EXTRACTION ORDER	EIGENVALUE	RADIANS	CYCLES	GENERALIZED MASS	GENERALIZED STIFFNESS
1	170	1.077513E 06	1.038033E 03	1.652081E 02	6.327703E-04	6.817642E 02
2	171	1.983351E 06	1.408315E 03	2.241403E 02	5.648492E-04	1.120294E 03
3	169	3.864545E 06	1.965944E 03	3.128738E 02	4.677235E-04	1.807538E 03
4	168	9.303013E 06	3.050084E 03	4.854360E 02	7.598657E-04	7.441160E 03
5	167	1.093243E 07	3.306422E 03	5.262334E 02	7.904069E-04	8.641062E 03
6	166	1.787291E 07	4.227633E 03	6.728486E 02	1.171202E-03	2.093280E 04
7	165	2.003565E 07	4.476117E 03	7.123962E 02	5.203013E-04	1.042457E 04
8	164	2.062640E 07	4.541629E 03	7.228228E 02	8.001572E-04	1.650436E 04
9	163	2.969723E 07	5.44[illegible] 03	8.673467E 02	8.172584E-04	2.427195E 04
10	162	3.212414E 07	5.667812E 03	9.020605E 02	5.339344E-04	1.715218E 04
11	161	4.484128E 07	6.696357E 03	1.065759E 03	0.0	0.0
12	160	4.668794E 07	6.832855E 03	1.087483E 03	0.0	0.0
13	159	4.734200E 07	6.880551E 03	1.095074E 03	0.0	0.0
14	158	4.873609E 07	6.981187E 03	1.111091E 03	0.0	0.0
15	157	6.143741E 07	7.838199E 03	1.247488E 03	0.0	0.0
16	156	6.38001[illegible] 07	7.9[illegible]500E 03	1.2[illegible]1250E 03	0.0	0.0
17	155	7.40562[illegible] 07	8.605590E 03	1.369622E 03	0.0	0.0
18	154	7.40585[illegible] 07	8.605723E 03	1.369644E 03	0.0	0.0
19	153	8.79[illegible] 07	9.10[illegible]684E 03	1.449851E 03	0.0	0.0
20	152	8.3768[illegible] 07	9.152535E 03	1.456671E 03	0.0	0.0
21	151	1.0[illegible] 08	1.004[illegible] 04	1.599374E 03	0.0	0.0
22	150	1.09876[illegible] 08	1.047982E 04	1.667915E 03	0.0	0.0
23	149	1.12287[illegible] 08	1.059656E 04	1.686496E 03	0.0	0.0
24	148	1.17876[illegible] 08	1.085707E 04	1.727956E 03	0.0	0.0
25	147	1.240[illegible] 08	1.113803E 04	1.772673E 03	0.0	0.0
26	146	1.24792[illegible] 08	1.118000E 04	1.779353E 03	0.0	0.0
27	145	1.34354[illegible] 08	1.159115E 04	1.844790E 03	0.0	0.0
28	144	1.35419[illegible] 08	1.163683E 04	1.852059E 03	0.0	0.0
29	143	1.415061E 08	1.189563E 04	1.893249E 03	0.0	0.0
30	142	1.496004E 08	1.223114E 04	1.946647E 03	0.0	0.0
31	141	1.594057E 08	1.262556E 04	2.009423E 03	0.0	0.0
32	140	2.008252E 08	1.417124E 04	2.255429E 03	0.0	0.0
33	139	2.0[illegible] 08	1.43826[illegible] 04	2.289067E 03	0.0	0.0
34	138	2.218637E 08	1.489509E 04	2.370627E 03	0.0	0.0
35	137	2.446493E 08	1.564127E 04	2.489385E 03	0.0	0.0
36	136	2.676630E 08	1.636041E 04	2.603840E 03	0.0	0.0
37	135	2.689091E 08	1.639845E 04	2.609874E 03	0.0	0.0
38	134	2.845691E 08	1.686918E 04	2.684813E 03	0.0	0.0
39	133	2.894531E 08	1.701332E 04	2.707754E 03	0.0	0.0
40	132	3.116815E 08	1.765450E 04	2.809802E 03	0.0	0.0
41	131	3.487398E 08	1.867993E 04	2.973004E 03	0.0	0.0
42	130	3.761577E 08	1.939479E 04	3.086776E 03	0.0	0.0
43	129	4.664762E 08	2.160732E 04	3.438912E 03	0.0	0.0
44	128	4.920279E 08	2.218170E 04	3.530328E 03	0.0	0.0
45	127	6.838976E 08	2.615143E 04	4.162129E 03	0.0	0.0
46	126	8.274355E 08	2.876518E 04	4.578117E 03	0.0	0.0
47	125	8.833787E 08	2.972168E 04	4.730352E 03	0.0	0.0
48	124	1.282669E 09	3.581437E 04	5.700031E 03	0.0	0.0
49	123	1.332790E 09	3.650739E 04	5.810332E 03	0.0	0.0
50	122	1.614683E 09	4.018312E 04	6.395340E 03	0.0	0.0

EIGENVALUE 1.077513E 06

REAL EIGENVECTOR NO. 1

POINT ID.	TYPE	T1	T2	T3	R1	R2	R3
1	G	1.233363E-04	1.233408E-04	1.674953E-01	-2.332935E-01	2.332922E-01	0.0
2	G	1.109969E-04	6.504753E-05	3.394654E-01	-1.654689E-01	4.594985E-01	0.0
3	G	5.770195E-05	5.769805E-05	6.836808E-01	-3.228186E-01	3.229135E-01	0.0
4	G	6.504639E-05	1.109500E-04	3.394623E-01	-4.594979E-01	1.658911E-01	0.0
5	G	8.163092E-05	1.553322E-04	6.377049E-03	-2.821397E-01	1.646640E-03	-7.251982E-03
6	G	1.457794E-04	1.750828E-04	5.955305E-03	-1.355569E-01	7.096797E-03	-1.435082E-02
7	G	1.992790E-04	1.992992E-04	5.532976E-03	-9.881894E-04	9.883093E-04	1.147326E-07
8	G	1.750788E-04	1.457965E-04	5.955331E-03	-7.096231E-03	1.355582E-01	1.435100E-02
9	G	1.553391E-04	8.364153E-05	6.377108E-03	-1.646067E-03	2.821438E-01	7.252555E-03
10	G	1.482294E-04	0.0	6.539334E-03	0.0	3.433944E-01	0.0
11	G	1.075139E-04	0.0	4.109331E-01	0.0	5.537450E-01	0.0
12	G	5.586832E-05	0.0	8.265212E-01	0.0	3.901860E-01	0.0
13	G	0.0	0.0	9.999122E-01	0.0	0.0	0.0
14	G	0.0	5.586242E-05	8.265185E-01	-3.901953E-01	0.0	0.0
15	G	0.0	1.075030E-04	4.109251E-01	-5.537426E-01	0.0	0.0
16	G	0.0	1.482112E-04	6.539244E-03	-3.433852E-01	0.0	0.0
17	G	0.0	-1.306382E-01	6.344479E-03	-9.408132E-02	0.0	0.0
18	G	-2.495667E-05	-1.064943E-01	6.218154E-03	-7.473302E-02	0.0	5.540512E-02
19	G	-4.838820E-05	-4.621013E-02	5.903509E-03	-2.987140E-02	0.0	7.467043E-02
20	G	-7.279567E-05	-7.294385E-05	5.592706E-03	-2.939113E-03	2.839092E-03	-3.546122E-09
21	G	-4.953207E-05	-4.952657E-05	2.862908E-03	-2.467401E-03	2.467392E-03	-2.997693E-09
22	G	-2.426586E-05	-2.426482E-05	8.121009E-04	-1.521584E-03	1.521580E-03	-1.814442E-09
23	G	0.0	0.0	0.0	0.0	0.0	0.0
24	G	-4.621033E-02	-4.838262E-05	5.903535E-03	0.0	2.987088E-02	-7.967120E-02
25	G	-1.086495E-01	-2.409434E-05	6.219210E-03	0.0	7.473201E-02	-9.540613E-02
26	G	-1.308391E-01	0.0	6.344527E-03	0.0	9.408051E-02	0.0
27	G	-1.038691E-01	0.0	6.004062E-03	0.0	-9.930128E-02	0.0
28	G	-8.279341E-02	-5.551231E-05	5.916179E-03	0.0	-8.123571E-02	-4.793201E-02
29	G	-3.338908E-02	-1.170810E-04	5.706146E-03	0.0	-3.957918E-02	-6.109735E-02
30	G	-1.992979E-04	-1.992970E-04	5.535979E-03	8.283086E-03	-9.282606E-03	1.810913E-06
31	G	-1.170821E-04	-3.339186E-02	5.706126E-03	3.957634E-02	0.0	6.110030E-02
32	G	-5.551342E-05	-8.279818E-02	5.916130E-03	8.122981E-02	0.0	4.793353E-02
33	G	0.0	-1.038746E-01	6.004002E-03	9.929478E-02	0.0	0.0
34	G	0.0	5.941338E-02	5.859669E-03	1.037081E-01	0.0	0.0
35	G	-6.209146E-06	4.710201E-02	5.747806E-03	8.483565E-02	0.0	-2.800673E-02
36	G	-2.453044E-05	1.859141E-02	5.453039E-03	4.221701E-02	0.0	-3.514566E-02
37	G	-9.572196E-05	-5.592641E-05	5.104702E-03	1.205366E-02	-1.205507E-02	3.922876E-06
38	G	1.859103E-02	-2.852842E-05	5.453061E-03	0.0	-4.221941E-02	3.515343E-02
39	G	4.711394E-02	-6.204086E-06	5.747854E-03	0.0	-8.483940E-02	2.801202E-02
40	G	5.942736E-02	0.0	5.859736E-03	0.0	-1.037120E-01	0.0
41	G	1.582689E-01	0.0	5.872078E-03	0.0	-5.320346E-03	0.0
42	G	1.270116E-01	-1.970314E-04	5.673401E-03	0.0	-5.672846E-03	7.056367E-02
43	G	5.297021E-02	-4.608776E-04	5.104691E-03	0.0	-6.427474E-03	9.183437E-02
44	G	-8.742786E-04	-8.742767E-04	4.157964E-03	-1.107507E-03	1.109645E-03	1.985195E-06
45	G	-2.432231E-04	-2.432178E-04	2.656568E-03	-8.153191E-04	3.169310E-04	1.471984E-06
46	G	9.616866E-05	9.617055E-05	1.485437E-03	-5.026087E-04	5.037209E-04	9.825017E-07
47	G	1.646509E-04	1.646511E-04	6.136897E-04	-2.354099E-04	2.359556E-04	4.986652E-07
48	G	0.0	0.0	0.0	0.0	0.0	0.0
49	G	-4.668829E-04	5.296642E-02	5.104698E-03	6.434880E-03	0.0	-9.182787E-02
50	G	-1.970415E-04	1.270008E-01	5.673319E-03	5.678531E-03	0.0	-7.055610E-02

51	G	0.0	1.582525E-01	5.871966E-03	5.321205E-03	0.0	0.0
52	G	0.0	-2.290947E-04	6.024066E-03	-3.427513E-01	0.0	0.0
53	G	0.0	-2.020777E-04	4.106569E-01	-5.546569E-01	0.0	0.0
54	G	0.0	-1.134722E-04	8.266767E-01	-3.902253E-01	0.0	0.0
55	G	0.0	0.0	1.000000E 00	0.0	0.0	0.0
56	G	-1.135041E-04	0.0	8.266768E-01	0.0	3.901322E-01	0.0
57	G	-2.020869E-04	0.0	4.106771E-01	0.0	5.546986E-01	0.0
58	G	-2.291188E-04	0.0	6.024234E-03	0.0	3.427904E-01	0.0
59	G	-2.470077E-04	-2.753159E-04	5.760852E-03	-2.300653E-03	2.819394E-01	-3.407726E-03
60	G	-3.632398E-04	-4.977102E-04	5.053859E-03	-6.212439E-03	1.396132E-01	2.561223E-03
61	G	-5.963214E-04	-5.963703E-04	4.347466E-03	-4.957665E-03	4.943244E-03	-6.016757E-07
62	G	-4.976674E-04	-3.632708E-04	5.053949E-03	-1.396196E-01	6.725459E-03	-2.560282E-03
63	G	-2.752686E-04	-2.463821E-04	5.760722E-03	-2.819228E-01	2.302686E-03	3.408592E-03
64	G	-1.682442E-04	-2.193908E-04	3.393211E-01	-4.600865E-01	1.655598E-01	0.0
65	G	-1.240234E-04	-1.237986E-04	6.831726E-01	-3.226517E-01	3.235753E-01	0.0
66	G	-2.194332E-04	-1.[illegible]39E-04	3.393223E-01	-1.656314E-01	4.600468E-01	0.0
67	G	-3.017939E-04	-3.018198E-04	1.676397E-01	-2.335284E-01	2.335783E-01	0.0